A microfluidics study of surfactant flooding at optimum and under-optimum conditions

***Maazen Saarig**, Delft University of Technology*
*Thesis committee: **Dr. P.L.J. Zitha** (TU Delft, supervisor), **Dr. G. Bertotti** (TU Delft), **Dr. W.R. Rossen** (TU Delft), **Dr. M.T.G. Janssen** (TU Delft, daily supervisor)*
MSc thesis will be defended on Wednesday January 29, 2020 at 3.00 PM

Abstract

This paper investigates surfactant flooding using a microfluidic device. Its purpose is to validate the results obtained in recent core experiments reported by Janssen et al. (2019) and provide mechanistic interpretation. In these experiments authors injected a surfactant slug into sandstone cores, initially brought to residual oil saturation. Low oil/water IFT leads to oil mobilization and the formation of emulsions. Furthermore, authors found that oil is more effectively mobilized when the injected surfactant is at optimum salinity. In this study the following experiments are subsequently conducted in a microfluidic device to validate this optimum surfactant slug: primary drainage, waterflooding and surfactant flooding. In case of the surfactant flooding experiment, the micro-emulsion formation was observed at 1.5 PV and 1.25 PV for the under-optimum and optimum conditions respectively. In both conditions, an increased oil mobilization was obtained, compared to the waterflooding experiment. However, the optimum condition, with a slug salinity of 2.0 wt% NaCl outperformed the under-optimum condition with a slug salinity of 0.4 wt% NaCl in terms of oil recovery. The increased salinity in case of the optimum condition results in an lower IFT compared to the under-optimum condition, which in turn results in an higher capillary number. The obtained results indicate a dependency between the capillary number and the amount of oil droplets. The optimum capillary number can be found at the lowest oil saturation with the largest amount of droplets. Based on the results obtained from the conducted experiments on this microfluidic device, upscaling is considered to be a viable and educated recommendation.

1. Introduction

Primary and secondary oil recovery methods extract 15-40% of the oil initially in place (OIIP) (Schlumberger 2019). Oil gets trapped during immiscible oil displacement by water due to rock and geological properties. The overall recovery can be estimated by the product of the displacement efficiency and volumetric sweep efficiency. Displacement efficiency, depending on the ratio of the viscous forces to the capillary forces (capillary number), can be described as the fraction of oil that has been recovered from the swept region (Green and Willhite 1998).

Enhanced Oil Recovery (EOR) aims to optimize oil recovery or equivalently to minimize residual oil in the reservoir. Mobilization of trapped oil occurs when viscous or gravity forces exceed capillary forces (Morrow 1979). EOR uses different techniques or approaches, such as, chemical flooding, polymer flooding and gas injection (Lake 1989).

Chemical EOR methods aim to increase the displacement and/or volumetric sweep efficiency, resulting in increased oil recovery. The displacement efficiency can be increased by lowering oil/water interfacial tension (o/w IFT). The volumetric sweep efficiency on the other hand depends mainly on the mobility ratio between the displaced and the displacing phases along with the heterogeneity of the reservoir (Craig 1971).

Surfactant flooding is a chemical EOR method, in which the surfactant in aqueous solution reduces oil to water interfacial tension or o/w IFT (Holm and Robertson 1981). The mixture of oil, water and surfactant can be described based on different phase behaviors, where Winsor-I is the under-optimum, Winsor-II is the over-optimum and Winsor-III is the optimum salinity system (Winsor 1947). The Winsor-I system is a system where surfactant forms an oil-in-water emulsion in the aqueous phase, which is not favorable for lowering the IFT. In the Winsor-II system, the surfactants form water-in-oil emulsions in the oil phase, which is also unfavorable for EOR. In the Winsor-III system the surfactant forms a micro-emulsion in a separate phase between the oil and aqueous phases. In contrast to the previous systems, this phase behavior is ideal for EOR (Schlumberger 2019). Surfactant slug systems with an optimum salinity result in the lowest o/w IFT, which in turn leads to an improved displacement efficiency (Sheng 2010). The optimum salinity may also differ for core experiments due to its dependence on the concentration of the surfactants in the slug. Furthermore, the optimum salinity depends on the oil and surfactant type (Janssen et al. 2019).

Residual oil after waterflooding consists of relatively large blobs and ganglia (Janssen et al. 2019; Howe et al. 2015). Surfactant slug injection lowers the o/w IFT, thus inducing the mobilization of the residual oil. Pore level mechanism responsible for the partly mobilization of the residual oil after waterflooding includes IFT lowering, mobilizing ganglia and solubilizing remaining oil (Janssen et al. 2019). After the surfactant slug injection, residual oil consists most likely of primarily small oil droplets due to the mobilization. At the slug front multiple mobilized droplets coalesce leading to the formation of one larger droplet. i.e. the coalescence could be between mobilized droplets or mobilized and trapped oil droplets (Wasan et al. 1979; Rossen 1996). The remainder of the oil droplets, present in the slug, may form a micro-emulsion upstream of the oil bank.

Several studies describe the oil bank formation in the cores (Guo et al., 2012) Adrianov et al., 2012; Hosseini Nasab et al. 2015; Janssen et al. 2019). The formation of the oil bank was established using CT scanning, but core floods did not allow its direct visual observation. This should be validated by experiments at microscale, allowing one to understand the mechanisms of the formation of the oil bank. Prior research (Hurkmans 2017) on microscale has been done for polymer flooding, where the residual oil saturations similar to those measured in core floods were realized.

The objective of this study was to investigate the flow behavior of the surfactant slug in an oil filled microfluidic device and to compare it to core-scale models. In order to meet this objective, the study was organized in the following tasks:

- Quantify residual oil saturation and oil recovery after primary drainage, waterflooding and surfactant flooding
- Visualize the residual oil as a function of surfactant slug salinity
- Quantify the oil recovery as a function of salinity
- Examine the displacement behavior in a microfluidic device
- Visualize the oil bank formation, micro-emulsion and the solubilization of oil

2. Experimental

2.1 Materials and methods

2.1.1 Chemicals

The brine, prepared with NaCl (≥ 99% purity), has a concentration of 2.0 wt% in case of under-optimum conditions and 4.0 wt% in case of optimum conditions. The oil used in the experiments, n-hexadecane ($CH_3(CH_2)_{14}CH_3$) (≥ 99% purity), is combined with 0.065 wt% Nile red ($C_{20}H_{18}N_2O_2$ (≥ 99% purity)) serving as the fluorescent dye. When excited by wavelength within the range of 559-637 nm, oleic Nile red solution emits a red color (Greenspan et al. 1985). The solubility of Nile red in hexadecane tends to be 0.001 wt% (Yow and Routh 2008). However, to keep an optimized fluorescent effect, the higher concentration of 0.065 wt% is used. IOS2024, supplied in an active matter (AM) content of 19 wt%, was used as a IFT-reducing surfactant. In case of under-optimum conditions, a combination of 1 wt% sodium carbonate Na_2CO_3 (≥ 99% purity), 0.5 wt% sec-butanol $C_4H_{10}O$, 0.4 wt% sodium chloride (NaCl), and 0.3 wt% surfactant IOS2024 was used as the surfactant slug. For the optimum conditions, the surfactant slug consisted of a combination of 1 wt% sodium carbonate Na_2CO_3 (≥ 99% purity), 0.5 wt% sec-butanol $C_4H_{10}O$, 2 wt% sodium chloride (NaCl), and 0.3 wt% surfactant IOS2024. Butanol is used as a co-solvent to maintain the stability of the slug, whereas Hirasaki et al. (2011) concluded that the use of this co-solvent is not necessary when working with IOS2024 below 60 °C (Janssen et al. 2019). The study of Hirasaki et al. indicates that the molecular structure ensures sufficient stability, so the co-solvent is added to be consistent in terms of prior experiments in order to make a correlation between them (Janssen et al. 2019). **Table 1** provides an overview of the above mentioned chemical and fluid concentrations. The flushing and cleaning of the microfluidic device is performed by using CO_2. Nitrogen (N_2) is used in the backpressure in order to increase the pressure in the microfluidic device. This increased pressure will create a favorable environment for the CO_2 to dissolve in brine.

Table 1: Chemicals and fluids used per stage in the microfluidic experiments

	Primary imbibition	**Primary drainage**	**Waterflooding**	**Surfactant flooding**
Under-optimum	2.0 wt % NaCl	n-hexadecane, with 0.065 wt% Nile Red Dye	2.0 wt % NaCl	1.0 wt% Na_2CO_3 0.5 wt% $C_4H_{10}O$ 0.4 wt% NaCl 0.3 wt% IOS2024 surfactant
Optimum	4.0 wt% NaCl	n-hexadecane, with 0.065 wt% Nile Red Dye	4.0 wt% NaCl	1.0 wt% Na_2CO_3 0.5 wt% $C_4H_{10}O$ 2.0 wt% NaCl 0.3 wt% IOS2024 surfactant

2.1.2 Microfluidic device

The properties of the microfluidic device which is used in the experiments can be found in **Table 2**. The porosity of the microfluidic device is calculated using ImageJ software, considering only the area within the blue box shown in **Figure 2**. This clear framework of boundaries is chosen in order to prevent overestimation of the porosity by ImageJ software. The software will include the red shaded section in as porosity, while this section does not contain any pores or grains. The permeability (k) of the microfluidic device used in this research is 0.72 D ± 0.02. This value is estimated by taking the slope of the graph, which can be found in **Appendix B**. One of the reasons for this low permeability can be assigned to the very small inlet structure of the microfluidic device (**Appendix B**). Relatively high pressures are necessary to guarantee fluid flow through the very small inlet structure. Also the pore throats are not uniformly distributed and the sizes of the pores and pore throats are not constant along the width and length of the microfluidic device. The pore size distribution was determined and resulted in a nominal Gaussian distribution (**Appendix B**). The design of the chip and a chosen target area of the experiments at ~ 0.75 PV is shown in **Figure 1**. Flooding at 0.75 PV means that the invading fluid just touched the target area.

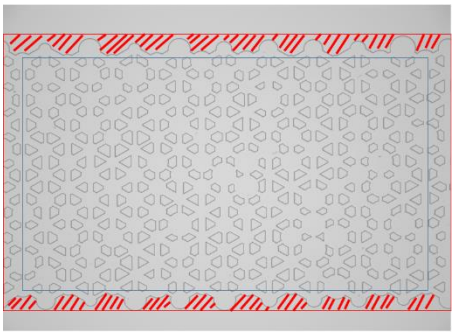

Figure 2: Porosity cut-off for quantification

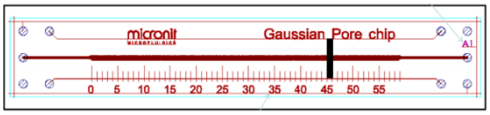

Figure 1: The design of the microfluidic device, with location of the target area marked by the black vertical bar

Table 2: The properties of the microfluidic design

Dimensions micromodel (mm)	**Constants**
Length	90
Width	15
Upper plate depth	1.1
Lower plate depth	0.70
Dimensions pore structure (mm)	
Length	60
Minimum width	0.013
Height	0.0050
Porosity (%)	71 ± 2.31
Permeability (D)	0.72 ± 0.02
PV (mm^3)	0.17 ± 0.002

2.2 Experimental Setup

The setup is shown schematically in **Figure 3.** It consists of three pumps (Harvard Apparatus: Ultratm 4400 Programmable Syringe Pump) which were used for injecting the following three liquids separately: oil, water and surfactant. Corresponding Hamilton 1800 series glass syringes of 100 or 250 µl were connected to the micro-fluidic device using a set of tubing and valves. Pressure transducers (Druck ATEX, with a range between 0-10 bar and an accuracy of ± 0.2%) were used to monitor the inlet and outlet pressures. The temperature is measured by the K-thermocouple (with an accuracy of ± 2.2°). The backpressure is connected to the outlet of the microfluidic device and the CO_2 cylinder is connected to the first valve. The latter one is necessary for flushing the whole system. A microscope (Leica DMi8 DFC7000) is used to grab images of the microfluidic device. This microscope operates with both transmitted (TL) and incident light (IL). Both TL and IL were used in the experiments, for contrast and good visualization respectively. The IL works best with a filter and therefore the TXR filter is used to tune to the range of wavelengths that is emitted by the Nile Red dye. This filter shows a black color for the matrix and water, while a red color is shown for the oil. The images in this study are captured by using a fluorescence camera (Leica DFC7000T). It is a built-in camera in the microscope and captures images of a resolution of 1920 x 1440.

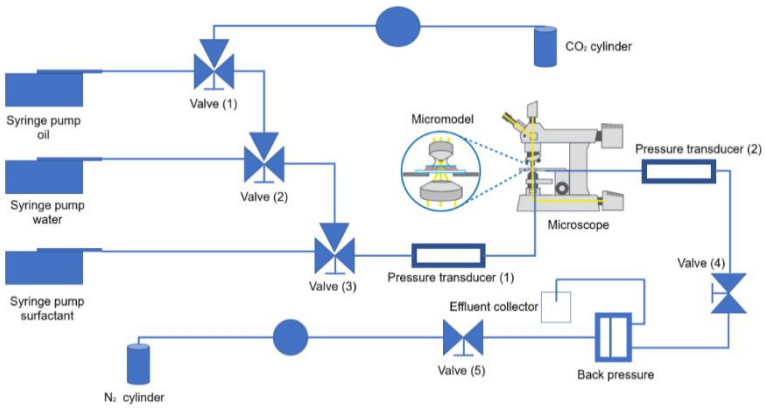

Figure 3: Experimental set-up used to perform microfluidic experiments

2.3 Experimental Procedure

The experimental procedure used in this study can be found in **Table 3.** The microfluidic device is flushed with CO_2 for 30 minutes at an injection pressure of 5 bar. This is performed to ensure removal of air and to achieve full saturation of the chip with CO_2. Next, the chip is flushed with brine for 20 PV and the outlet pressure is kept at 10 bar to let the CO_2 dissolve completely. The absolute permeability will be determined by varying the flowrate using Darcy's Law (Darcy 1856). Then, oil (n-hexadecane) is injected for 4 PV. Next, a bump flood of 40 nl/min is executed. After primary drainage, brine is injected for the next step (waterflooding), with a flowrate of 4 nl/min for 4 PV. Waterflooding is then finished with a bump flood of 40 nl/min for 1 PV. Finally, surfactant flooding is applied with different flowrates: Under-optimum 1 (UO-1) with 1.4 nl/min, Under-optimum 2 (UO-2) with 4 nl/min and Optimum 1 (O-1) with 4 nl/min. These flowrates are chosen as such that the interstitial velocities of the microfluidic device are similar to those in the core-flooding experiments (Janssen et al. 2019).

Table 3: Sequence of experimental procedures and properties

Step	Description	Backpressure (bar)	Flowrate (nl/min)	Injection Pressure (bar)
1	CO_2 flushing	-	-	5.0
2	Brine saturation	10		-
2.1	Perm. determination	-	change flowrate	-
3	Oil injection			
3.1	Primary drainage	-	4.0	-
3.2	Bump flood	-	40	-
4	Waterflooding			
4.1	Imbibition	-	4.0	-
4.2	Bump flood	-	40	-
5	Surfactant injection	-	UO-1: 1.4 UO-2: 4.0 O-1: 4.0	-

2.3.1 Cleaning procedure

After every experiment the microfluidic device was flushed with propanol for cleaning off the surfactants, oil, brine and unfavorable particles, such as dust. Afterwards, the microfluidic device is placed in a vacuum oven to dry. It is then placed in a beaker of ethanol, which is put in an ultrasonic bath, so the remaining particles are removed. Then, it is dried again in the vacuum oven to get rid of any remaining liquids or gases.

Even after this intensive cleaning procedure, the following two cases can occur: 1. Remaining particles observed under the microscope. 2. System is oil-wet and the Nile red dye is sticking to the walls of the pore structure.

In case of 1, Acetone is used for flushing the system or as a replacement for the ethanol in the ultrasonic bath.

In case of 2, the system is flushed with toluene; which leads to a more water-wet system and dissolving the Nile red dye. However, toluene should not remain in the system, hence the system is flushed with ethanol and demineralized water afterwards.

3.Results and Discussion

The goal of this research is to present, compare and explain the behavior of surfactant flooding under two different conditions, the under-optimum and optimum salinity conditions. The most important factor that will be compared, is the so called oil recovery factor (R_F). This section will start with presenting the results of the surfactant flooding experiments under the above mentioned conditions, followed by a comparison between the results of the two conditions. Afterwards, a comparison will be made between EOR experiments and literature.

During this study, many experiments were proposed, but not all of them were successfully conducted. A list of all experiments can be found in **Appendix A.**

3.1 Under-Optimum Conditions

As discussed in the section **Experimental Procedure**, the Under-Optimum condition consists of two distinct cases during the surfactant flooding phase, i.e. UO-1 and UO-2.

For both cases, the oil saturation (S_o) of the target area during primary drainage, waterflooding and surfactant flooding is visualized. The corresponding amount of PV injected and the oil saturation in percentage are also included.

3.1.1 Primary Drainage and Waterflooding

During the primary drainage and waterflooding stages within the UO-1 case, the flowrate of 4.0 nl/min and the amount injected of 5PV are kept constant**. Figure 4** shows the oil saturation in case of UO-1 and UO-2 after primary drainage, while **Figure 5** shows the oil saturation for both cases after waterflooding. The average oil saturation S_o in both cases after primary drainage are quite close to each other and the same can be said about the S_o in both cases after waterflooding. This implies that the conducted experiments can be considered to be reliable.

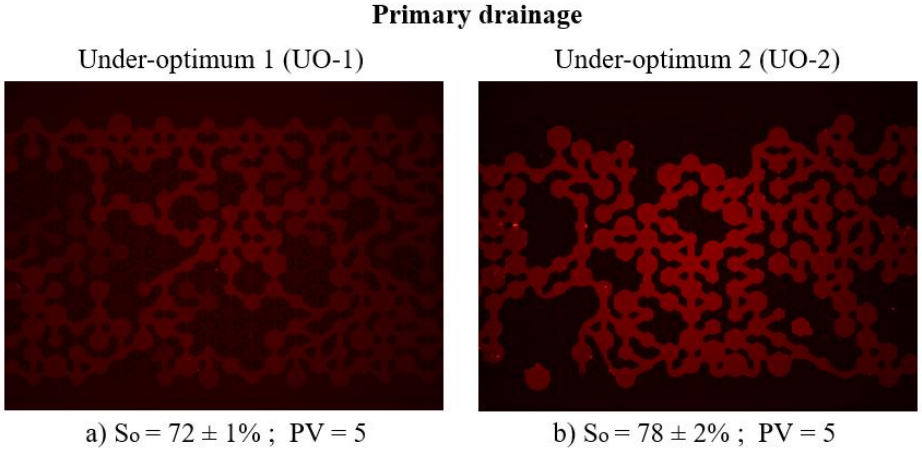

Figure 4: : Target area after primary drainage in case of UO-1 and UO-2

The structure of the oil, after primary drainage, looks like a connected chain that forms one large body. After waterflooding, several small disconnections of this chain can be observed.

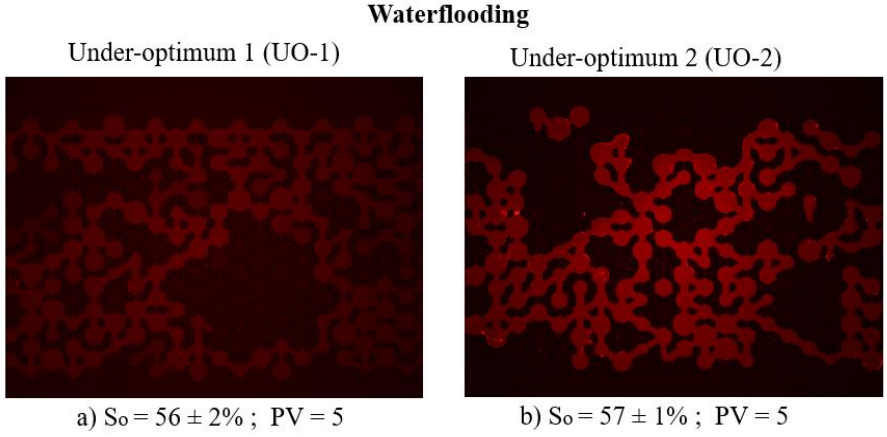

Figure 5: Target area after waterflooding in case of UO-1 and UO-2

3.1.2 Surfactant flooding

During surfactant flooding with a flowrate of 1.4 nl/min, injected PV is increased in order to visualize the process of micro-emulsion creation. This micro-emulsion creation and the displacement behavior of the surfactant, can also be derived from the figures. In case of UO-1, even with an injection amount of 2 PV, no mixture of oil, water and surfactant can be seen, see **Figure 6**. The figure shows only randomly distributed oil blobs along the target area, implying an absence of micro-emulsion formation. This is also the reason why no figures with lower PV's are shown, since they do not differ from the one with PV of 2.

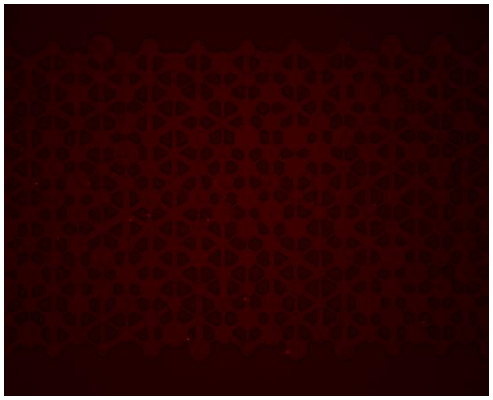

So = 15 ± 5% ; PV = 2

Figure 6: Target area surfactant flooding UO-1

This lead to the introduction of UO-2 case, in which the flow rate is increased to 4.0 nl/min to achieve micro-emulsion creation. **Figure 7** , which shows the results of UO-2. The micro-emulsion formation starts to be visible from a PV of 1.5.

The above mentioned chain shows significantly larger discontinuities after the surfactant starts to touch the target area with an injection amount of 0.75 PV. This results into the formation of a large amount of small sized oil droplets, due to the lowering of the IFT.

An increase of the oil saturation is measured between 0.75 PV and 1.25 PV, see **Figure 7.a** and **Figure 7.b**. This increase is actually unwanted, but not unexpected. The increase is due to oil mobilization upstream of the target area and is entering the target area after the surfactant flooding has started. The oil can be trapped by the inlet or tubing which in turn can move into the chip. This results in a higher oil saturation during the experiments.

The creation of micro-emulsion can be seen at 1.5 PV and is also visible at 1.75 PV, see **Figure 7.c** and **Figure 7.d** respectively. A trend can be seen regarding the light intensity; an increase in injected surfactant amount, expressed in PV, results into a decrease of the light intensity. The low light intensity in case of UO-1 is due to the duration of the experiment, while the decrease of the light intensity in case of UO-2 is because of the micro-emulsion formation.

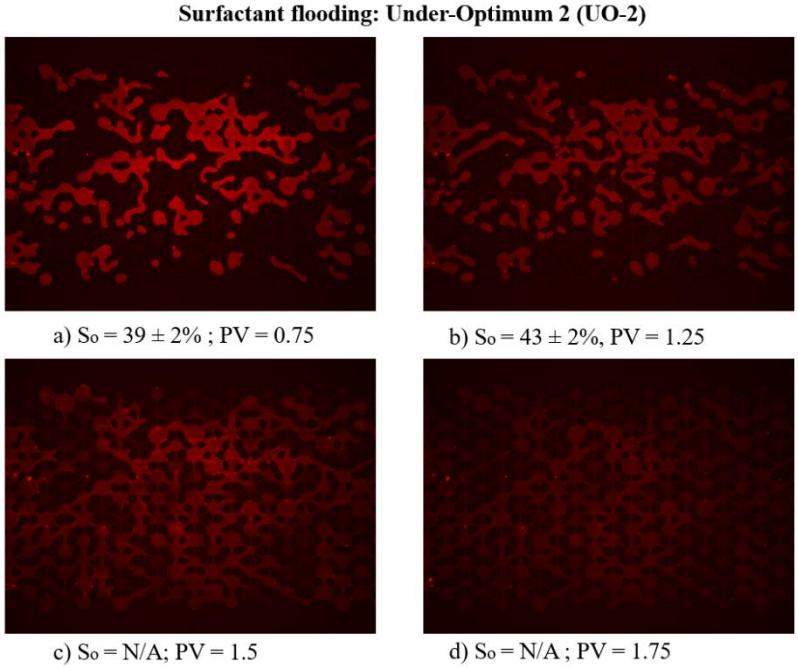

Figure 7: Target area during surfactant flooding UO-2

3.2 Optimum Conditions

The salinity of the surfactant slug of 0.4 wt% NaCl in the Under-Optimum conditions is increased to 2.0 wt% NaCl in the Optimum conditions. The increase of the salinity until 2.0 wt% NaCl leads to an optimum decrease of the IFT, which results in improved displacement efficiency of the oil. However, it also means that the viscosity of the brine will decrease slightly and thus increasing the mobility ratio. This eventually will result in a decrease of the sweep efficiency. This effect combined with the wettability change shall result in a fingering displacement behavior.

3.2.1 Primary Drainage and Waterflooding

Figure 8 shows the oil saturation after primary drainage and waterflooding in case of the Optimum conditions (O). As discussed above, oil saturation after primary drainage and waterflooding in Optimum and Under-Optimum conditions are similar. Also a similar formation of a large body of oil can be observed, while the displacement behavior shows dissimilarities. In case of O, the water is trapped by oil due to the change in wettability from water- to oil-wet. This change of wettability also explains the observance of more oil at the edges of the pore structure in case of O relative to UO. The wettability change can be indirectly explained by the difference in contact angles between the grains and the fluids, see **Appendix B**.

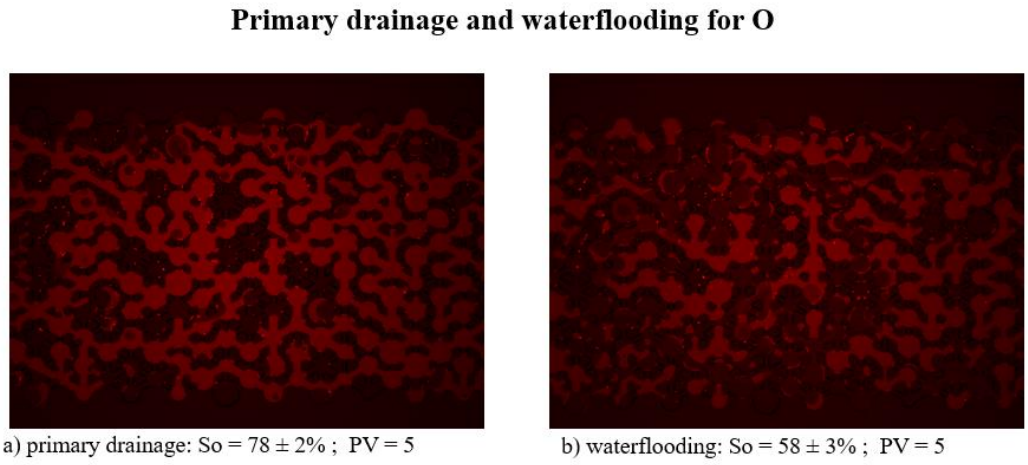

Figure 8: Target area after primary drainage and waterflooding O

The graph in **Figure 9** represents a comparison of oil recovery factor between the O and UO conditions during waterflooding. The x-axis presents the PV injected [-], while the y-axis shows the oil recovery factor [-] obtained from the experiments. Between 0 PV and 1 PV , the recovery factor in all conditions is increasing from 0 up to a certain value. After 1 PV, there is a breakthrough and stoppage of oil mobilization. Even with a bump flood after 4 PV, no extra oil mobilization can be observed. This is due to the fact that water flows in the most preferred flow paths and if that is already saturated by water, there is no more recovery of oil (Lyons & Plisga 2011).

It must be stated that the recovery factor after waterflooding should actually be the same for all experiments. This is clearly not the case in **Figure 9,** but this discrepancy can be the result of sensitivity of the system in terms of temperature and pressure. Also the viscosity and wettability differences could explain this difference.

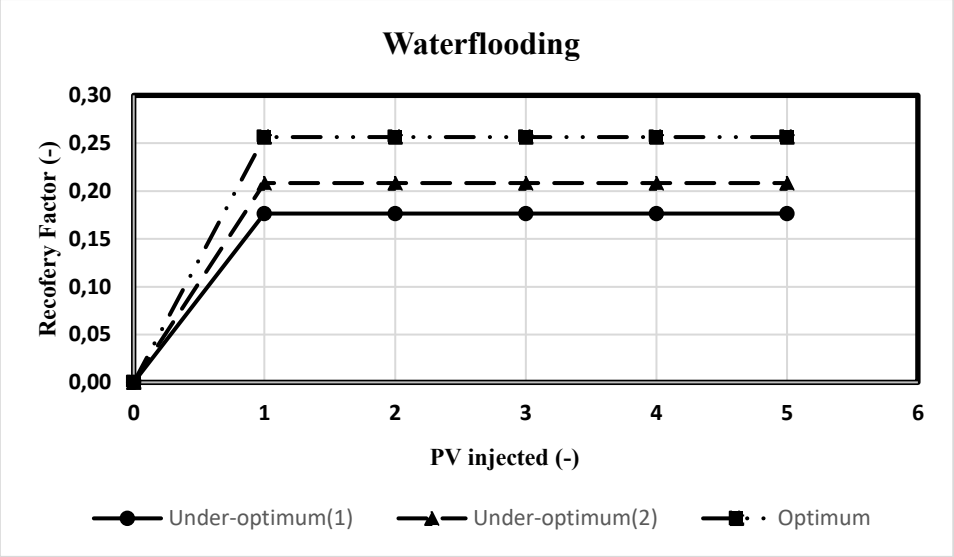

Figure 9: Oil recovery after waterflooding for under- and optimum conditions

3.2.2 Surfactant Flooding

Figure 10 shows the oil saturation during the surfactant flooding in case of the Optimum conditions. The results show more smaller oil droplets relative to UO under the same PV injected. An important observation is the occurrence of micro-emulsion creation that takes place under a lower PV injected (1.25) compared to UO (1.5 PV).

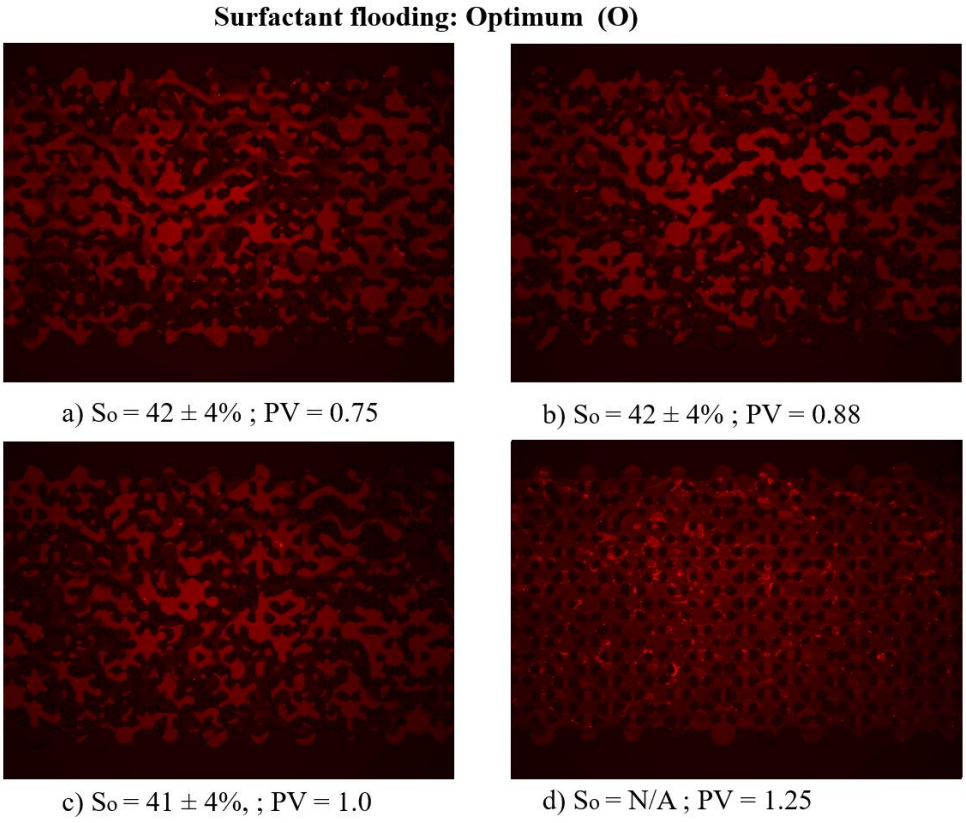

Figure 10: Target area during surfactant flooding O

Figure 11 shows the oil saturation after 2 PV surfactant injection for UO-2 and O conditions. It can be seen that the oil saturation for the O condition is smaller and the droplets are also relatively smaller to the UO case. There is no sign of the micro-emulsion for the O case, while for the UO-2 case there is some visible evidence for the existence of micro-emulsion in the middle of the target area. The injected amount of 2 PV is not common in cores or reservoirs, but gives a better explanation about the break-up of the micro-emulsion after intensive flooding.

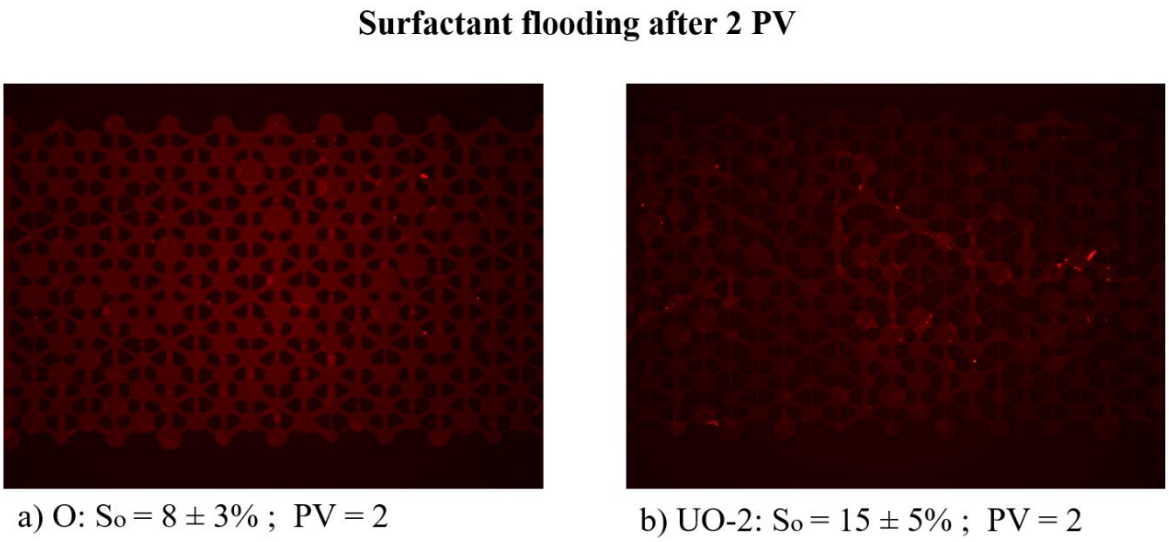

Figure 11: Target are after 2 PV surfactant flooding for O and UO-2

Figure 12 represents a comparison of oil recovery factor (R_F) between the O and UO conditions during surfactant flooding. It can be observed that for the Optimum conditions the oil recovery is always higher than for the Under-Optimum conditions. Between 0.75 PV and 1.0 PV, the R_F in case of the Under-Optimum conditions is decreasing, while the R_F in case of the Optimum conditions stays relatively constant. After 1.0 PV, the R_F in O starts to increase, while the R_F in UO still decreases until the PV of 1.25 is reached. The decreasing of the R_F in UO, can be explained due to oil mobilization upstream of the target area as well as the entering of the oil just after the surfactant flooding has started. The oil can be trapped by the inlet or tubing, and during the experiments the oil can move into the chip, giving a higher oil saturation.

It is most likely that this happened for the optimum conditions as well, preventing a higher slope of the R_F line in O.

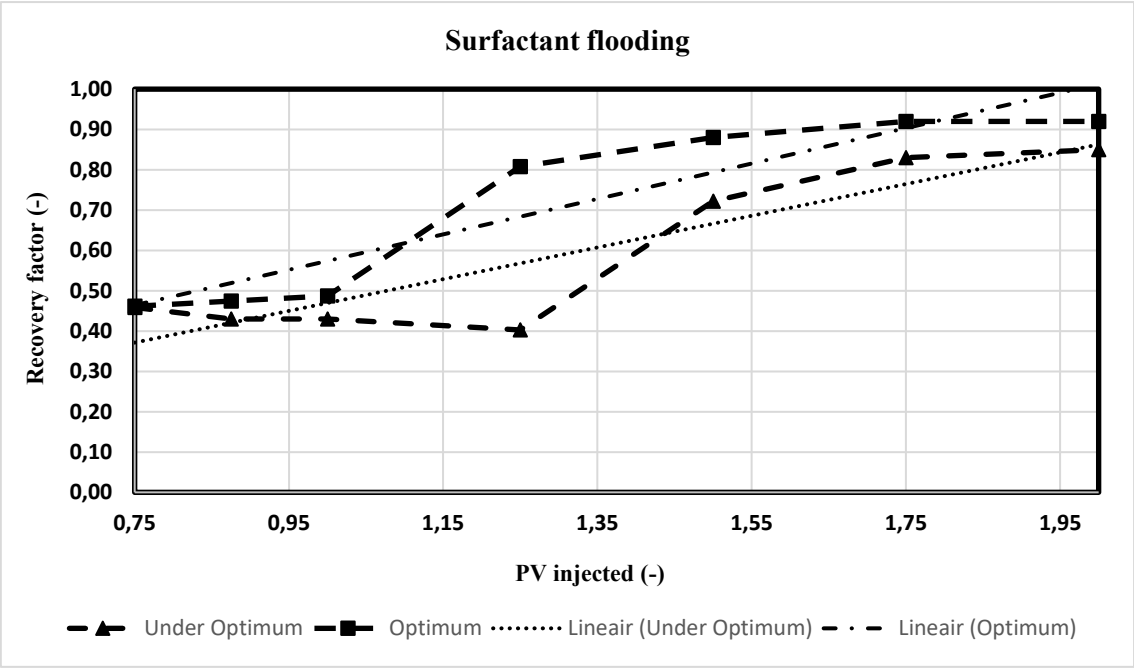

Figure 12: The oil recovery after surfactant flooding for under-optimum and optimum conditions

3.3 Capillary number

The calculation of the capillary number is done by the following equation: $N_c = \frac{v\,\mu}{IFT}$, where N_c is the capillary number, μ the viscosity, v the velocity and *IFT* the interfacial tension. The IFT that has been used for the calculations, were obtained from Janssen et al. (2019). The oil and brine that has been used for these experiments are almost similar to Janssen et al. (2019).

The relationship between the capillary number and the number of oil droplets divided by the oil saturation is graphed in **Figure 13.** The graph shows an increase in the number of oil droplets relative to the oil saturation when the capillary number (N_c) is increased. In case of surfactant flooding the residual oil contains smaller droplets relative to waterflooding between 0.75 and 1.0 PV for both experimental conditions (UO and O). However, the droplet sizes are significantly smaller in case of O compared to UO. This is because of the low o/w IFT that is breaking up the oil structure. From this we can derive the following relationship: the lower the IFT, the smaller the droplets. This is inline with what was expected and is shown in **Figure 13.**

An optimum result is obtained from a combination of a high number of droplets and low oil saturation.

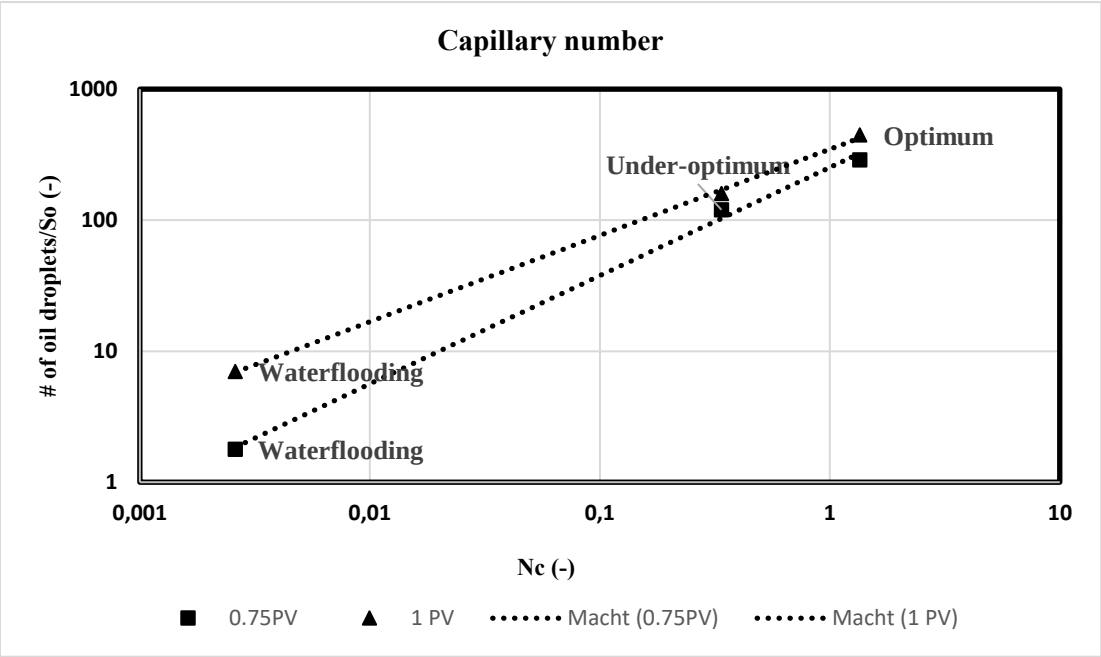

Figure 13: The relationship between Nc and the oil droplets

3.4 Experiments vs Literature

Under stable displacement conditions primary drainage and waterflooding in cores are consistent with Buckley-Leverett theory (Buckley and Leverett, 1942). The frontal displacement of primary drainage in the microfluidic device is shown in **Figure 14**, in which the displacement front is highlighted in black. It can be seen that the displacement behavior in the microfluidic device is not piston-like, but more like a fingering displacement. This is due to the scale, the heterogeneity, bypass, trapped brine and preferable low resistant paths (Anbari et al. 2018). Also, Anbari et al. (2018) conclude that the wettability is a factor for the displacement efficiency and behavior. It was found that the increased wettability of the invading fluid could enhance the displacement until a critical contact angle. When this critical angle is surpassed, it will have a reversed effect on the enhancement. On a larger scale, for example cores, this effect is not visible and can be described as a piston-like displacement.

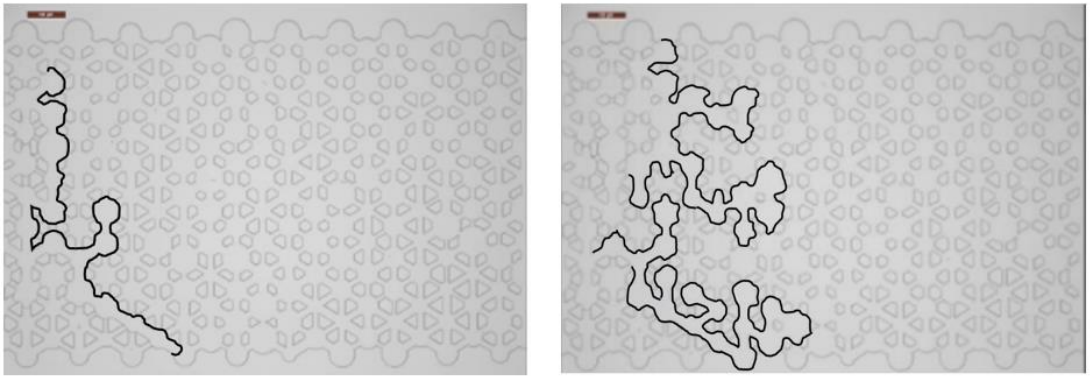

Figure 14: Frontal Displacement of primary drainage in micromodel

For higher velocities instead, it has been seen that there is indeed a piston-like displacement. These experiments are performed under significantly higher flowrates compared to this study. For higher flowrates, it is more likely to have a piston-like displacement, because of the ratio between the inertial and viscous forces is increasing, resulting in a more constant and laminar flow (Reynolds 1900). In this study a flowrate is used which is similar to the interstitial velocity in reservoir conditions.

If the oil recovery (0.18-0.26) results compared with the core flood experiments (0.39-0.42) (Janssen et al. 2019), it can be said that the oil recovery for water flooding is low. This can be due to the low permeability of the microfluidic device. Another important factor is the heterogeneity, in other words the distribution of the pores, which influences the permeability and subsequently the oil recovery. As mentioned before, the distribution of the pores in the microfluidic device has a nominal Gaussian distribution, resulting in a lower oil recovery.

The oil saturation along the chip, depicted in **Figure 15,** is distributed uniformly and is equivalent to the distribution of the core flood experiments of Janssen et al. (2019). A slight decrease of the oil saturation along the microfluidic device can be observed. However, this is an usual and expected behavior in this type of experiments. The capillary end effect, which appears in the core experiments, does not occur in the microfluidic device, hence it is not visible in graphs.

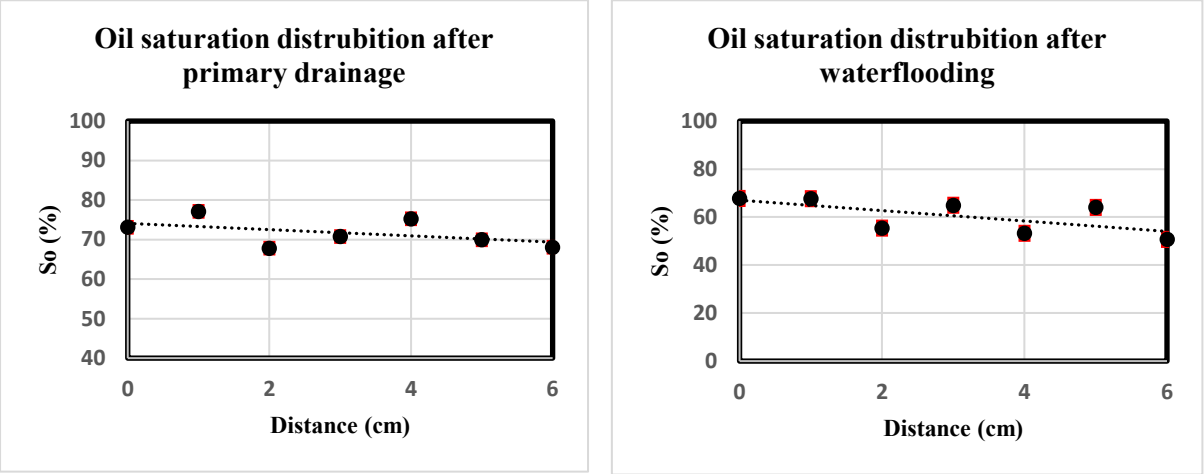

Figure 15: Oil distribution along the chip for primary drainage (left) and waterflooding (right)

For the Under-Optimum 2 and Optimum conditions, the micro-emulsion formation has been observed at 1.5 PV and 1.25 PV respectively. The micro-emulsion formation is observed due to the intensity of the red-color. However, it is almost impossible to determine the residual oil after the final formation of the micro-emulsion. Micro-emulsion formation in cores is not visible due to the scale, but it is possible to determine the oil saturation. So a combination of core and microfluidic device experiments provide the best understanding of the behavior of surfactant flooding.

There is no oil bank formation visible in all the experiments. However, in core experiments, the oil bank formation, is clearly visible, as schematically shown in **Figure 16**. The reason for both observations is the scale in which the experiments are conducted.

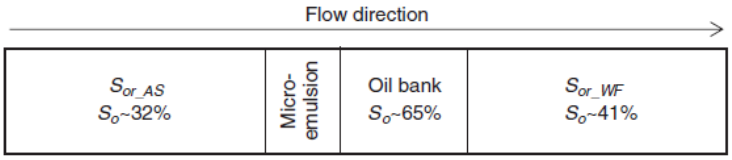

Figure 16: Schematic visualization of the fluid distribution after AS slug, obtained by Janssen et al. (2019)

In case of the microscale, the scale of target area is 1 millimeter, while for the core it is almost 1 meter. The coalescence of the oil droplets is also not visible in the microscale experiments, but it does actually occur. The proof of this occurrence is the observance of smaller droplets for the oil saturation after surfactant slug.

4. General discussion

The goal of this research was to investigate the flow behavior of surfactant flooding in a microfluidic device and to compare this to a core-scale model. This section stresses the differences in the pore structure between microfluidic device and granular porous medium. The main discussion is whether the conditions of this experimental study on the microfluidic device can be upscaled, i.e. can be applied in reservoirs.

The design of the microfluidic device, as can be seen in **Figure 1**, contains some dead volume. The dead volume is not being used for any calculation of the pore volumes and/or quantification of the oil saturation, however, it can have a large impact on the experiments. This is due to trapped oil/water inside these dead volumes. Just before the entrance of the pore structure it has a triangle shape, which effects the trapping more negatively. The entrance of the pore structure, as described earlier, consists of very small inlet tubes, resulting in a system that is sensitive to blocking or trapping. The pore structure itself, which has been discussed earlier in this paper, has a nominal Gaussian distribution. In this study a nominal Gaussian distribution affects the permeability and tortuosity undesirably. Especially when the used microfluidic device is compared to the Bentheimer cores. These Bentheimer cores have a different distribution (Peksa 2015), the peak of the graph is shifted to smaller diameters, which means that the Bentheimer core contains a larger faction of smaller diameters. The microfluidic device, with the pore structure included, has a 2½ D shape instead of 3D. In reservoirs and cores, the pores are three-dimensional. The displacement, tortuosity and the flow behavior in general are more complex. The microfluidic device is made of glass, which gives another solid-fluid interaction compared to a typical Bentheimer core or reservoir. The mineralogy and composition of Bentheimer can affect the flow and the oil distribution.

Let us now shed some light on the physical flow behavior in this study. The Nile Red dye causes a change in wettability, making it stick to the glass. This can be prevented by including acetone to the oil solution. This is due to the fact that Nile Red dye is soluble in acetone. However, in order to make comparison with the experiments of Janssen et al. (2019), this preventive measure is not used in the micro-scale experiments.

The flowrate has been increased after the first experiment. The reason for increasing the flowrate is to have a better understanding of the flow behavior and to see a creation of a micro-emulsion. Nevertheless, the higher used flowrate is normally not used in reservoirs or cores.

The capillary number is calculated using the IFT measurements of Janssen et al. (2019). The brine and surfactant are identical to those of Janssen et al. (2019). However, they used an oil, doped with 15 or 20 % dopant, instead of Nile Red dye. This extra substance has such a little weight percentage, that it can be assumed that the IFT measurements do not differ significantly.

The most important question remains whether it is possible to upscale the microfluidic device to core-scale and reservoir-scale. In this study differences and similarities between the microscale and the core- and reservoir-scale have come to light. The model does not have a one-on-one relationship with the core or the reservoir. The core and the reservoir are much more complex, but this is understandable since the micromodel is a simplification of these two. A lot of the assumptions made in core studies are confirmed or explained better due to microscale experiments. Some differences in terms of rock type, fluid composition, mineralogy, heterogeneity etc. that are present, also exist between a core and a reservoir.

However, with this kind of studies it is relatively easy to make a prediction or confirm a certain assumption. Because of this, the microfluidic device is a good way to check the reservoir-scale and then test the end result in the lab. By doing this, it is possible to alter the production strategy, in order to recover more oil. This can be done by e.g. changing the surfactant and thus getting an optimal condition

or by changing the brine composition, stopping it from getting different side effects. To conclude, the microfluidic device can be a proper tool in the petroleum sector, where it is important to recover as much oil as possible.

5. Conclusion

The main objective of this paper is to study the flow behavior of the surfactant slug in an oil filled microfluidic device and to compare them with core-scale models.

In the microfluidic device the salinity of the surfactant slug has correlations with the oil recovery, size and amount of the oil droplets and the general displacement behavior. These correlations are also observed in the previous mentioned core flood experiments. A surfactant slug with optimum salinity conditions injected into the microfluidic device has: 1: the highest oil recovery, 2: the smallest and most oil droplets, 3: the forming of micro-emulsions starting at less PV injected, 4: more fingering displacement.

The displacement behavior is not piston-like as described by Buckley and Leverett and observed in core floods. In microfluidic devices the displacement contains more fingering. The use of microfluidic device makes it possible to notice the location, time and PV injected of the micro-emulsion formation. In case of core-scale, the oil droplets can be seen, but the distinction between micro-emulsion or residual oil cannot be made. Coalescence of oil and oil bank formation were not visible due to the scale. Finally, it should be mentioned that the wettability changes the system in terms of displacement behavior and sweep efficiency.

6. Recommendations

- A new chip is designed to partly solve the problems of the trapped fluid that has been displaced in a different phase. This is shown in **Figure 17.**
- Foam after surfactant flooding is widely used in EOR and further research should be done on this scale.
- Glass with 3D pores should be used for a better understanding and to include complexity of the pores.
- Bentheimer microfluidic device has to be used to get the one-on-one comparison with a core.
- A simulation must be performed for the microfluidic device structures, in order to perform sensitivity analysis and to have an educated reasoning for eventual upscaling.

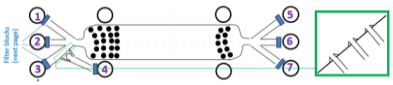

Figure 17: New design of the microfluidic device, obtained from Micronit (2019)

7. References

1. Anbari, Alimohammad, et al. "Microfluidic model porous media: fabrication and applications." *Small* 14.18 (2018): 1703575.
2. Buckley, Se E., and MCi Leverett. "Mechanism of fluid displacement in sands." *Transactions of the AIME* 146.01 (1942): 107-116.
3. Craig, Forrest F. *The reservoir engineering aspects of waterflooding*. Vol. 3. New York: HL Doherty Memorial Fund of AIME, 1971.
4. Darcy, Henry. "The public fountains of the city of Dijon." *Dalmont, Paris* 647 (1856).
5. Farajzadeh, Rouhollah, et al. "Foam–oil interaction in porous media: implications for foam assisted enhanced oil recovery." *Advances in colloid and interface science* 183 (2012): 1-13.

6. Green, Don W., and G. Paul Willhite. *Enhanced oil recovery*. Vol. 6. Richardson, TX: Henry L. Doherty Memorial Fund of AIME, Society of Petroleum Engineers, 1998.
7. Hirasaki, George, Clarence A. Miller, and Maura Puerto. "Recent advances in surfactant EOR." *SPE Journal* 16.04 (2011): 889-907.
8. Holm, L. W., and Steven D. Robertson. "Improved micellar/polymer flooding with high-pH chemicals." *Journal of Petroleum Technology* 33.01 (1981): 161-172.
9. Howe, Andrew M., et al. "Visualising surfactant enhanced oil recovery." *Colloids and Surfaces A: Physicochemical and Engineering Aspects* 480 (2015): 449-461.
10. Huang, David D., and Matt M. Honarpour. "Capillary end effects in coreflood calculations." *Journal of Petroleum Science and Engineering* 19.1-2 (1998): 103-117.
11. Hurkmans, M. J. E. J. "The Development of a Microfluidic device Protocol followed by a Study of Oil Mobilization in the Microfluidic device." (2017).
12. Janssen, Martijn TG, Pacelli LJ Zitha, and Rashidah M. Pilus. "Oil Recovery by Alkaline/Surfactant/Foam Flooding: Effect of Drive-Foam Quality on Oil-Bank Propagation." *SPE Journal* (2019).
13. Lake, Larry W. "Enhanced oil recovery." (1989).
14. Lyons, William C., and Gary J. Plisga. *Standard handbook of petroleum and natural gas engineering*. Elsevier, 2011.
15. Mavko, Gary, Tapan Mukerji, and Jack Dvorkin. *The rock physics handbook: Tools for seismic analysis of porous media*. Cambridge university press, 2009.
16. Morrow, Norman R. "Interplay of capillary, viscous and buoyancy forces in the mobilization of residual oil." *Journal of Canadian Petroleum Technology* 18.03 (1979).
17. Nasab, H. S. M., et al. "Mechanistic Modeling of Alkaline/Surfactant/Polymer Flooding Process at Under-Optimum Salinity Condition for Enhanced Oil Recovery." *Paper SPE 174641 Presented at the SPE Enhanced Oil Recovery Conference, KL, Malaysia, 11–13 August*. 2015.
18. Peksa, Anna E., Karl-Heinz AA Wolf, and Pacelli LJ Zitha. "Bentheimer sandstone revisited for experimental purposes." *Marine and Petroleum Geology* 67 (2015): 701-719.
19. Reynolds, Osborne, Arthur William Brightmore, and William Henry Moorby. *Papers on Mechanical and Physical Subjects: 1869-1882*. Vol. 1. The University Press, 1900.
20. Rossen, William R. "Foams in enhanced oil recovery." *Foams: Theory, Measurements and Applications* 57 (1996): 413-464.
21. Sheng, James. *Modern chemical enhanced oil recovery: theory and practice*. Gulf Professional Publishing, 2010.
22. "The Oilfield Glossary - Schlumberger Oilfield Glossary". *Glossary.Oilfield.Slb.Com*, 2019, https://www.glossary.oilfield.slb.com/.
23. Wasan, D. T., et al. "The role of coalescence phenomena and interfacial rheological properties in enhanced oil recovery: an overview." *Journal of Rheology* 23.2 (1979): 181-207.
24. Winsor, P.A. 1947. "Hydrotropy, solubilization and related emulsification processes." Trans. Faraday Soc. 376-398.
25. Yow, Huai Nyin, and Alexander F. Routh. "Release profiles of encapsulated actives from colloidosomes sintered for various durations." *Langmuir* 25.1 (2008): 159-166.

Appendix A

All conducted experiments are presented in this table. Also some failed experiments are presented for exemplary reasons.

Experiments:	Succeed/failed	Reason of failure
1	Failed	Leakage of the system
2	Failed	Leakage of the system
3	Failed	The inlet tube is blocked by particles (A1)
4	Failed	The inlet tube is blocked by particles (A1)
5	Succeed	-
6	Failed	Nile Red dye is blocking the entrance (A2)
7	Failed	Electricity shut down
8	Failed	Back flow occurred due to negative pressure drop (A5)
9	Succeed	-
10	Failed	Simultaneously injecting two fluids (A6)
11	Failed	System became oil wet. Nile red was sticking to the glass. First, it was not visible, but after primary imbibition, it was only visible with the microscope with the TXR filter. (A4)
12	Failed	Same as experiments 11
13	Failed	The concentration Nile Red Dye was too high to continue the experiment (A4)
14	Succeed	-

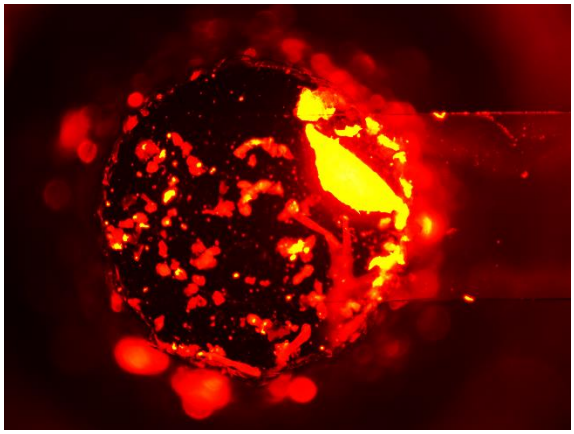

A1: The inlet of the micromodel is blocked by a particle that emits sharp light, assumed to be Nile Red dye.

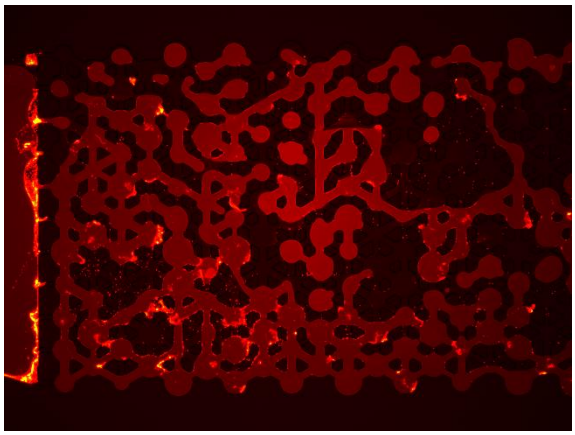

A2: High concentration of Nile Red dye and the entrance of the pore structure (left side). And this is blocking the fluid from flowing. Also it is visible that water is trapped in the upper inlet.

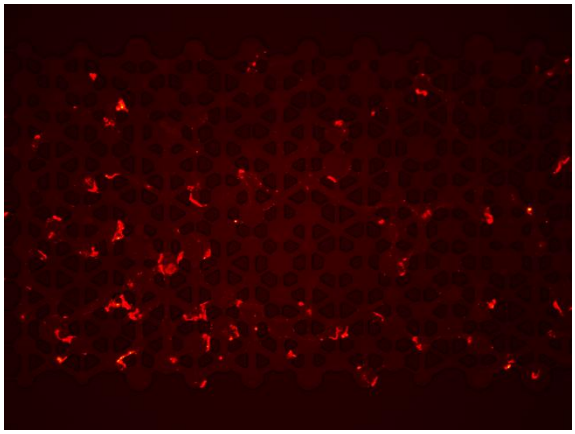

A3: Nile Red dye is sticking to the wall of the pores indicated in the brighter red colour.

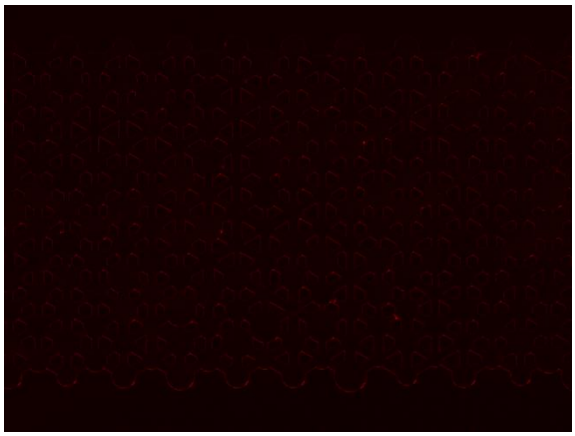

A4: System became oil wet, even after flushing. This is confirmed and seen as Nile Red dye sticking to the glass.

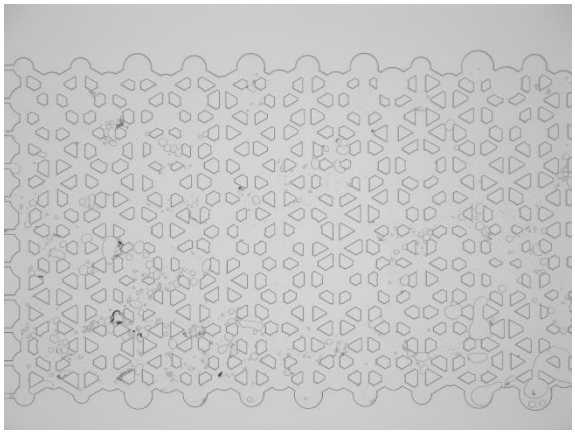

A5: Back flow occurred due to negative pressure drop. Seen as gas bubbles in the system. (small, light grey bubbles in the pores).The darker (almost black) parts represent dirt/dust or unfavourable parts.

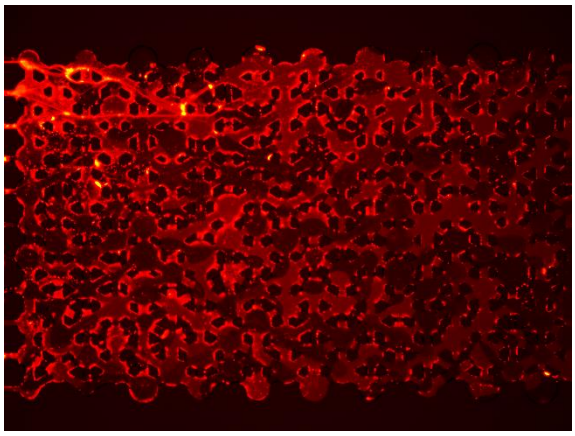

A6: At the top oil is injected, indicated by the red colour, while starting from approximately half-way down, water is injected which is indicated as black. This is a case where two fluids are being injected, which is unfavourable and thus unwanted. In this particular case, the experiment was not even usable.

Appendix B

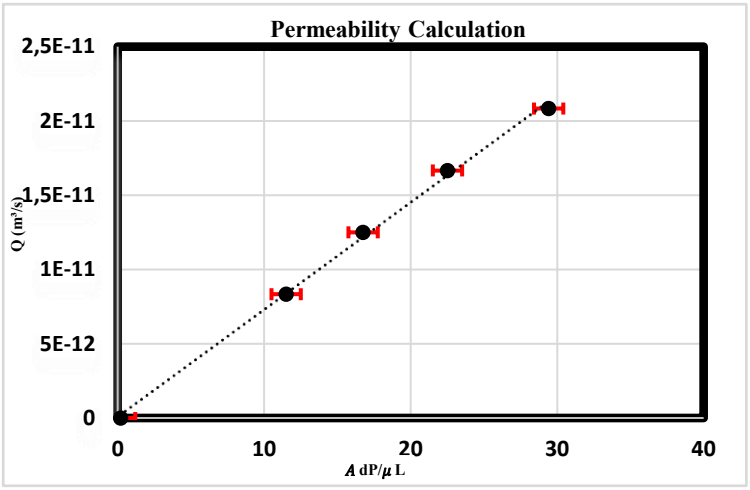

B1: Permeability calculation for the microfluidic device

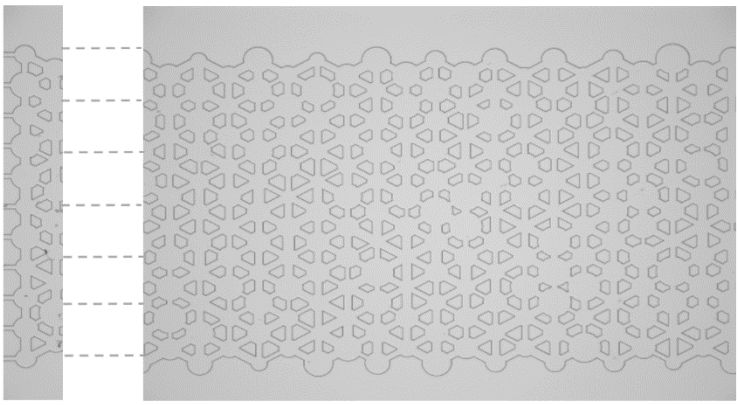

B2: inlet structure and pore structure of the microfluidic device

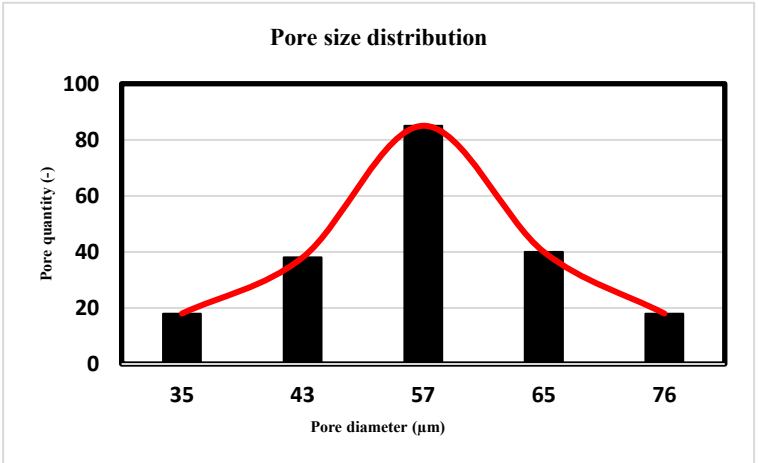

B3: Pore size distribution of the microfluidic device

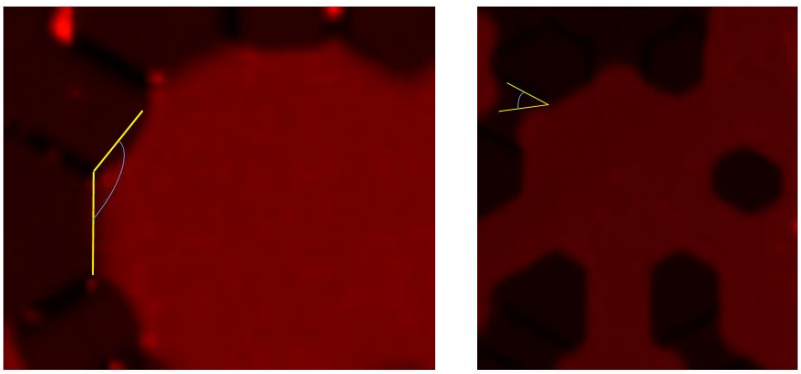

B4: Contact angles for O (left) and UO-2 (right), with 142 and 33 degrees respectively